MODELING SUPERCRITICAL CARBON DIOXIDE INJECTION IN

HETEROGENEOUS POROUS MEDIA

Christine Doughty*[1] and Karsten Pruess.[1]

ABSTRACT

We investigate the physical processes that occur during the sequestration of carbon dioxide (CO_2) in liquid-saturated, brine-bearing geologic formations using the numerical simulator TOUGH2. CO_2 is injected in a supercritical state that has a much lower density and viscosity than the liquid brine it displaces. In situ, the supercritical CO_2 forms a gas-like phase, and also partially dissolves in the aqueous phase, creating a multi-phase, multi-component environment that shares many important features with the vadose zone. The flow and transport simulations employ an equation of state package that treats a two-phase (liquid, gas), three-component (water, salt, CO_2) system. Chemical reactions between CO_2 and rock minerals that could potentially contribute to mineral trapping of CO_2 are not included. The geological setting considered is a fluvial/deltaic formation that is strongly heterogeneous, making preferential flow a significant effect, especially when coupled with the strong buoyancy forces acting on the gas-like CO_2 plume. Key model development issues include vertical and lateral grid resolution, grid orientation effects, and the choice of characteristic curves.

INTRODUCTION

The risks associated with increased concentrations of greenhouse gases in the atmosphere have prompted study of the feasibility of geological sequestration of carbon dioxide (CO_2) produced by power plants, refineries, and other industrial concerns that produce localized sources of CO_2. We investigate the physical processes that occur during the sequestration of supercritical CO_2 in liquid-saturated, brine-bearing geologic formations. Other potential sites for sequestration include coal beds and depleted oil and gas reservoirs. Among the motivations for using brine formations are their widespread availability and lack of competing uses. Brine formations associated with oil reservoirs often have the added advantages of being well characterized and in close proximity to CO_2 sources.

Several other recent studies (van der Meer, 1995; Pruess and García, 2002; Pruess et al., 2003) have also investigated CO_2 sequestration in brine formations, but they have all employed rather idealized representations of the geology. The present paper is part of an on-going effort to investigate the impact of geologic heterogeneity on the capacity of the subsurface to sequester CO_2, by incorporating realistic geologic variability in mathematical models of the subsurface (Doughty et al., 2001; Doughty et al., 2002; Knox et al., 2003). Here we focus on the effects of

[1] Earth Sciences Division, E.O. Lawrence Berkeley National Laboratory, #1 Cyclotron Rd., MS 90-1116, Berkeley, CA, 94720, U.S.A.

grid resolution, grid orientation, and characteristic curves (capillary pressure and relative permeability as a function of liquid saturation) in a strongly heterogeneous geologic setting in which buoyancy flow is significant. Although the application is two-phase flow in deep saturated formations, the model-development issues addressed are broadly applicable to multi-phase systems including the vadose zone.

FLOW AND TRANSPORT PROCESSES

We employ TOUGH2 (Pruess et al., 1999) with an equation of state package called ECO2, which treats a two-phase (liquid, gas), three-component (water, salt, CO_2) system in the pressure/temperature regime above the critical point of CO_2 ($P = 73.8$ bars, $T = 31^{\circ}$C). ECO2 is adapted from EWASG (Battistelli et al., 1997), which treats the same components under sub-critical conditions, and is designed for geothermal reservoir simulation. Properties of supercritical CO_2 are calculated from a computer program kindly provided to us by V. Malkovsky (private communication, 1999), that implements the correlations developed by Altunin (1975) on the basis of extensive laboratory investigations. Detailed comparison studies with experimental data and with more recent equation of state formulations have shown Altunin's correlations to be very accurate, typically agreeing to within 1 % or better with experimental data and with alternative correlations (García, 2003). Although ECO2 may include temperature variations, we use it in isothermal mode here.

Carbon dioxide is injected in a supercritical state that has a much lower density and viscosity than the liquid brine it displaces. In situ, the supercritical CO_2 partitions between an immiscible gas-like phase and dissolution in the aqueous phase, according to an extended version of Henry's Law, yielding a multi-phase, multi-component system. As in the vadose zone, strongly gravity-driven flow occurs and is very sensitive to geologic heterogeneity, leading to the potential for nominally vertical flow (liquid infiltration in the vadose zone, buoyant flow of CO_2 here) that is controlled by preferential flow paths. Also as in the vadose zone, the mobilities of the flowing phases depend strongly on multi-phase flow effects at the pore scale, as embodied in continuum-scale (i.e., model-scale) relative permeability functions that are often poorly known for a particular field site or fluid composition.

The present simulations are relatively short-term (less than 100 years), so they emphasize advective processes. Slower flow processes such as aqueous-phase diffusion of dissolved species and the buoyancy effect of dissolved CO_2 are not included. Salt may precipitate out of the brine, but the rock matrix itself is inert. Thus, chemical reactions between CO_2 and rock minerals that could potentially contribute to mineral trapping of CO_2 are not considered.

GEOLOGICAL SETTING AND MODEL DEVELOPMENT

The geological setting for our model is the fluvial/deltaic Frio formation in the upper Texas gulf coast (Galloway, 1982; Hovorka et al., 2001). We construct three-dimensional models stochastically, with model layers derived from three idealized representations of fluvial depositional settings found in this part of the Frio: barrier bars (continuous very high-permeability sands), distributary channels (intermingled sands and shales, with a large high-permeability sand component), and interdistributary bayfill (predominantly low-permeability discontinuous shale lenses, interspersed with moderate-permeability sand), as shown in Figure 1. Each depositional setting contains three facies, with the most prevalent one denoted the framework facies. The program TProGS (Carle and Fogg, 1996, 1997; Fogg et al., 2001) uses transition probability theory to construct multiple two-dimensional stochastic representations of

each depositional setting consistent with its idealized representation, as illustrated in Figure 2. Each realization honors the proportions, characteristic lengths, and juxtapositions of facies shown in Figure 1. Then, the vertical sequence of depositional settings within the model is assigned based on well log interpretation. In constructing the final three-dimensional model, one may either choose among the multiple realizations created for each depositional setting randomly, or pick them deliberately in order to reproduce realistic three-dimensional geologic structure. Here, we have used the latter method.
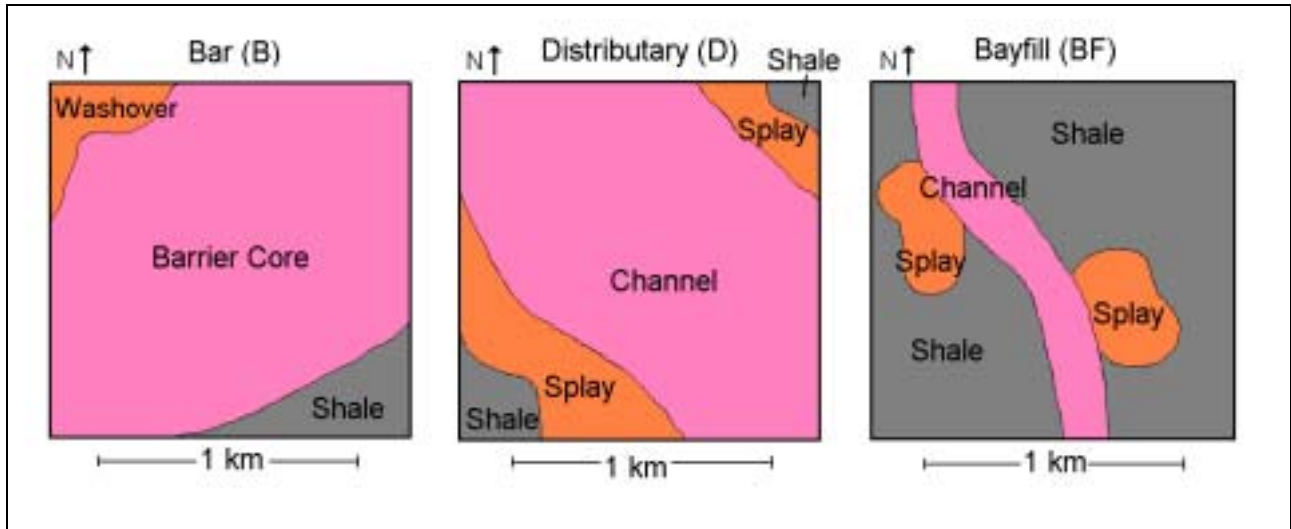

Figure 1. Idealized representations of three fluvial depositional settings found in the Frio formation, used by TProGS to generate stochastic permeability fields.
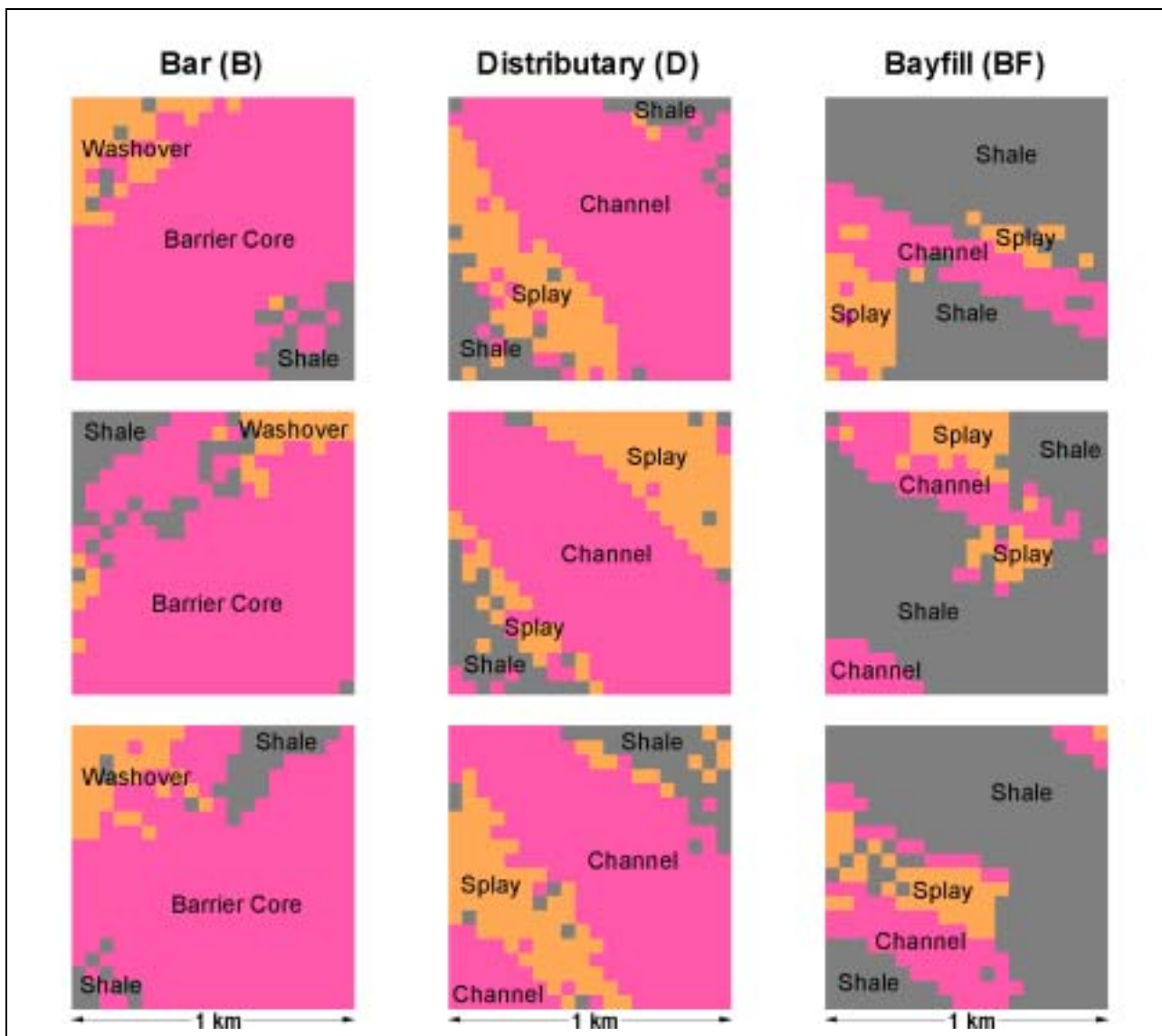
Figure 2. Examples of the stochastic realizations produced by program TProGS. Each column shows three of the ten realizations created for a given depositional setting.

Each facies corresponds to a material type in TOUGH2, and as such has its own set of flow properties. Overall, permeability varies by nearly six orders of magnitude among material types, making preferential flow a significant effect, especially when coupled with the strong buoyancy forces acting on the gas-like CO_2 plume.

Two TOUGH2 models have been developed. The first, the Umbrella Point model, is based on the well logs (Vining, 1997) shown in Figure 3. The model (Figure 4), is 1 km by 1 km by 100 m thick, and is intended to be roughly representative of the scale on which CO_2 from a single power plant might be stored. The model is bounded above and below by closed boundaries, which represent continuous shale layers. Lateral boundaries are open (constant-pressure), to represent natural spill points of the sequestration region. Within the model, several discontinuous bayfill layers exist that strongly retard and channel vertical flow. Table 1 summarizes the material properties used in the model, which are typical of nearby reservoirs in the Frio formation, but are not specific to the Umbrella Point site (Hovorka et al., 2001). Due to

a lack of data on two-phase flow properties of supercritical CO_2 and liquid brines, generic characteristic curves are used: van Genuchten (1980) for liquid relative permeability and capillary pressure and Corey (1954) for gas relative permeability.
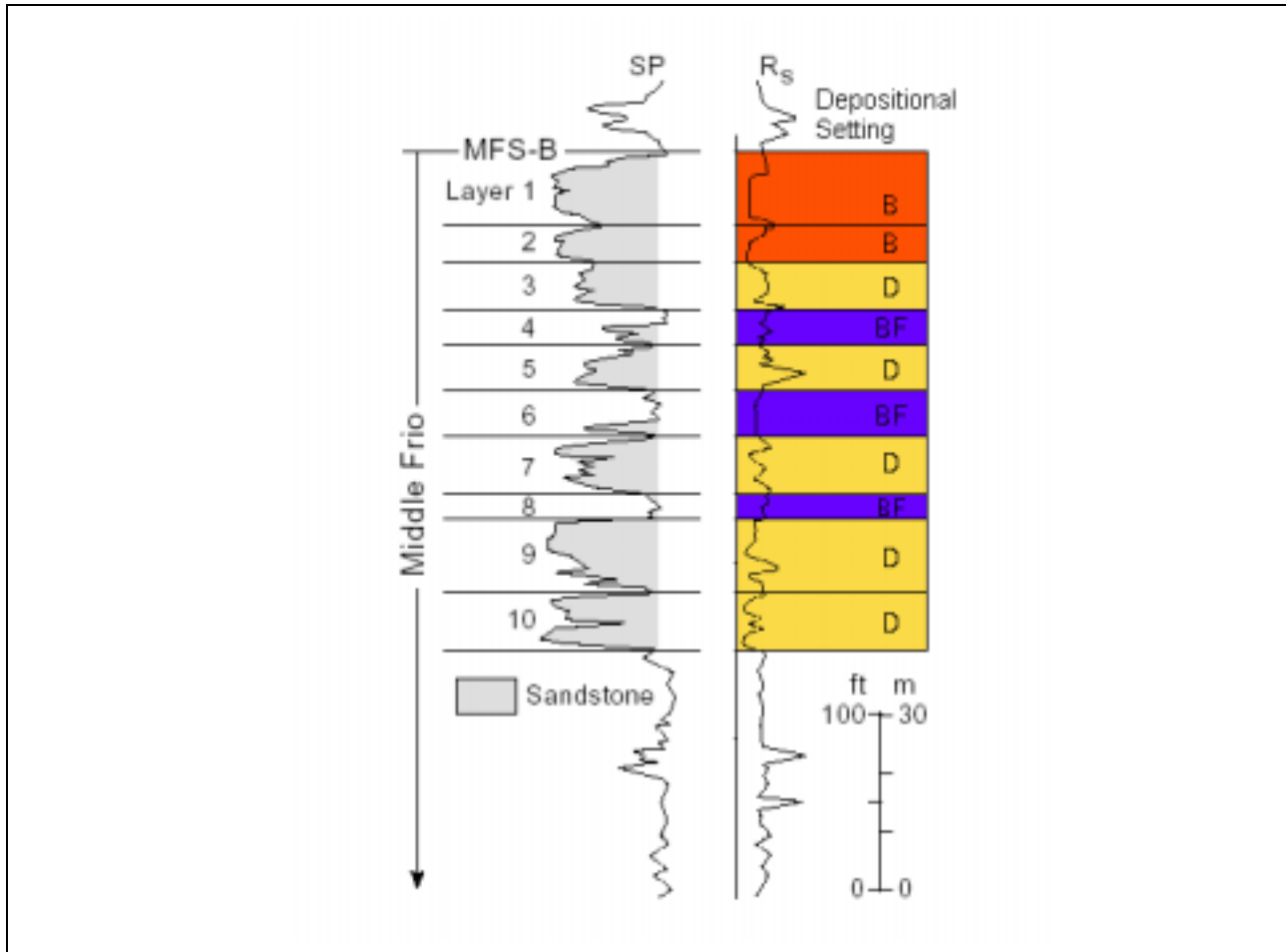

Figure 3. Well logs (Vining, 1997) and interpretation of sequence of depositional settings for Umbrella Point model (see Figure 4 for depositional-setting legend).

As in most three-dimensional model applications, we must balance the need for adequate model extent and spatial resolution with a computationally manageable number of grid blocks. The lateral constant-pressure boundaries provide a convenient way to limit the number of grid blocks, but are probably not the best way to conceptualize the sequestration volume boundary. A laterally extensive model has been created and although it is too cumbersome for routine use, it does confirm that the constant-pressure boundaries do not introduce significant errors to the CO_2 behavior within the 1 km by 1 km region (Doughty et al., 2002). Grid-block thicknesses vary with depth to resolve geologic layering, while the lateral grid spacing is uniform. In our basic grid (Figure 4), one model layer represents each of the ten depositional layers. Alternative grids that provide two or three model layers per depositional layer have also been constructed.

Note that the lateral model extent (1 km) is about the same as the characteristic length scale for geologic heterogeneity ($\sim$ 0.2 - 1 km, Figure 1), hence alternative stochastic realizations of the model may be expected to show markedly different flow and transport behavior. Two

additional versions of the basic model shown in Figure 4 have been developed, using the same sequence of depositional settings (Figure 3), but choosing different realizations for each layer.
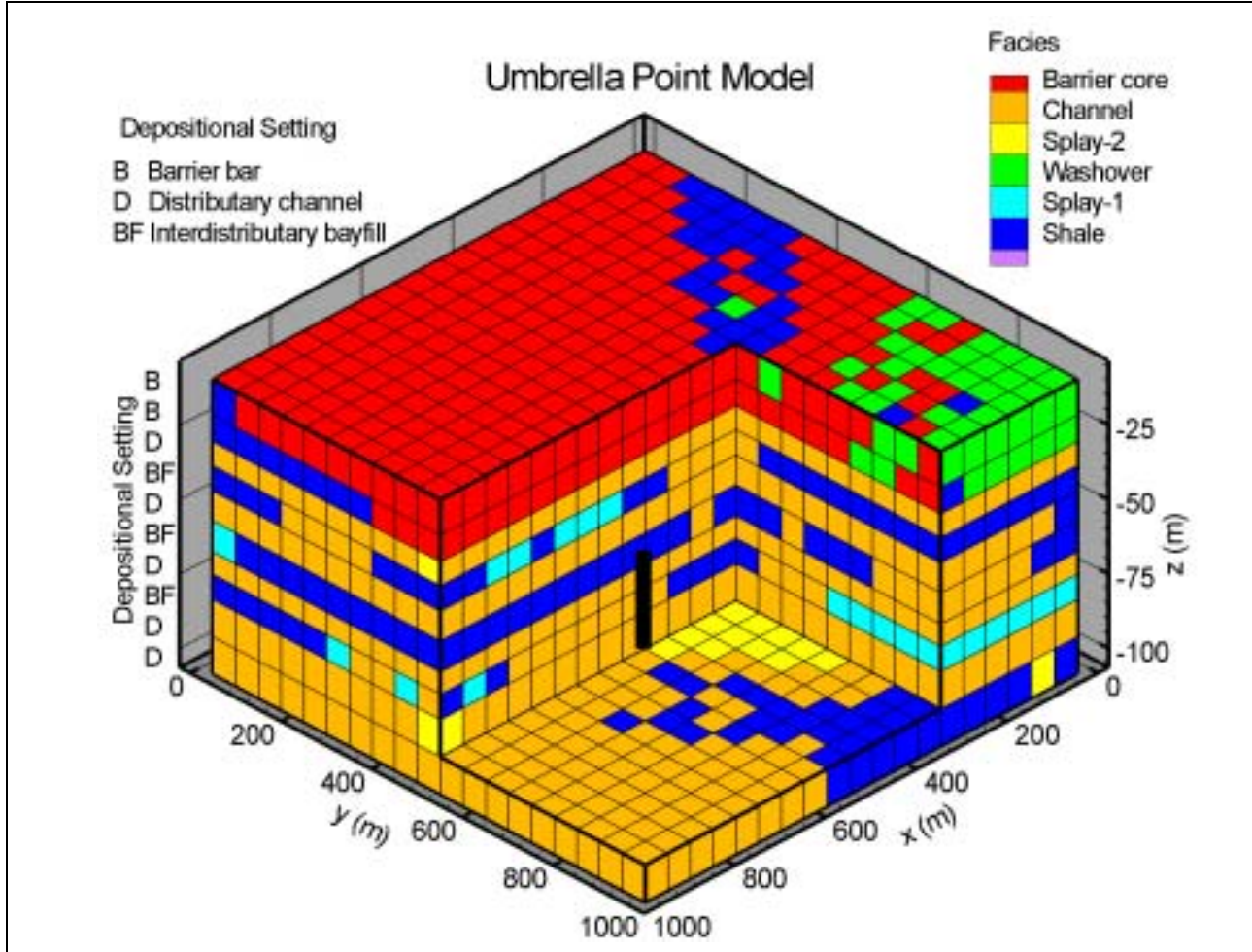
.

Figure 4. Cut-away view of Umbrella Point model. The injection well is shown as a black bar.

The second model (Figure 5) is 440 m by 440 m by 12 m thick, and represents the site of an upcoming pilot test of CO_2 sequestration in the Frio formation at the South Liberty field near Houston, Texas. As in the first model, closed upper and lower boundaries represent continuous shale layers, but in this model, three of the four lateral boundaries are also closed to represent the edges of a fault block. The idealized depositional settings shown in Figure 1 are used to generate depositional setting realizations and interpretation of local well logs (P. Knox, private communication, 2001) determines their sequence. The model includes three depositional settings, each composed of multiple grid layers. In the deepest depositional setting, an upward-coarsening sand, permeability varies with depth as well as facies. Table 2 summarizes the material properties used in the model, which are based on nearby Frio reservoirs (P. Knox, private communication, 2001). Our basic South Liberty model uses the same generic characteristic curves as the Umbrella Point model, but characteristic curves believed to be more representative of local conditions are also employed.

In the South Liberty model, vertical grid spacing varies to represent geology, and lateral grid spacing is also variable, with finer resolution around injection and monitoring well locations. Unlike the Umbrella Point model, which has horizontal layers, here layers dip at 15 degrees, with the open end of the model in the down-dip direction. Hence, buoyancy flow plays two important roles, moving CO_2 to the top of the formation and also up-dip toward the closed end of the fault block. The combination of these buoyancy-driven movements and the radial flow away from the injection well provides a challenge for a rectangular grid. Our basic model uses five-point differencing, but an alternative model using nine-point differencing for lateral connections has also been developed.

Figure 5 makes it clear that the lateral extent of the South Liberty model is comparable to the characteristic length scale for geologic heterogeneity, implying that as in the Umbrella Point model, alternative stochastic realizations of the model are likely to show markedly different flow and transport behavior. Thus far, only the model shown in Figure5 has been used for pilot-test simulations, but future work is planned to employ alternative realizations.
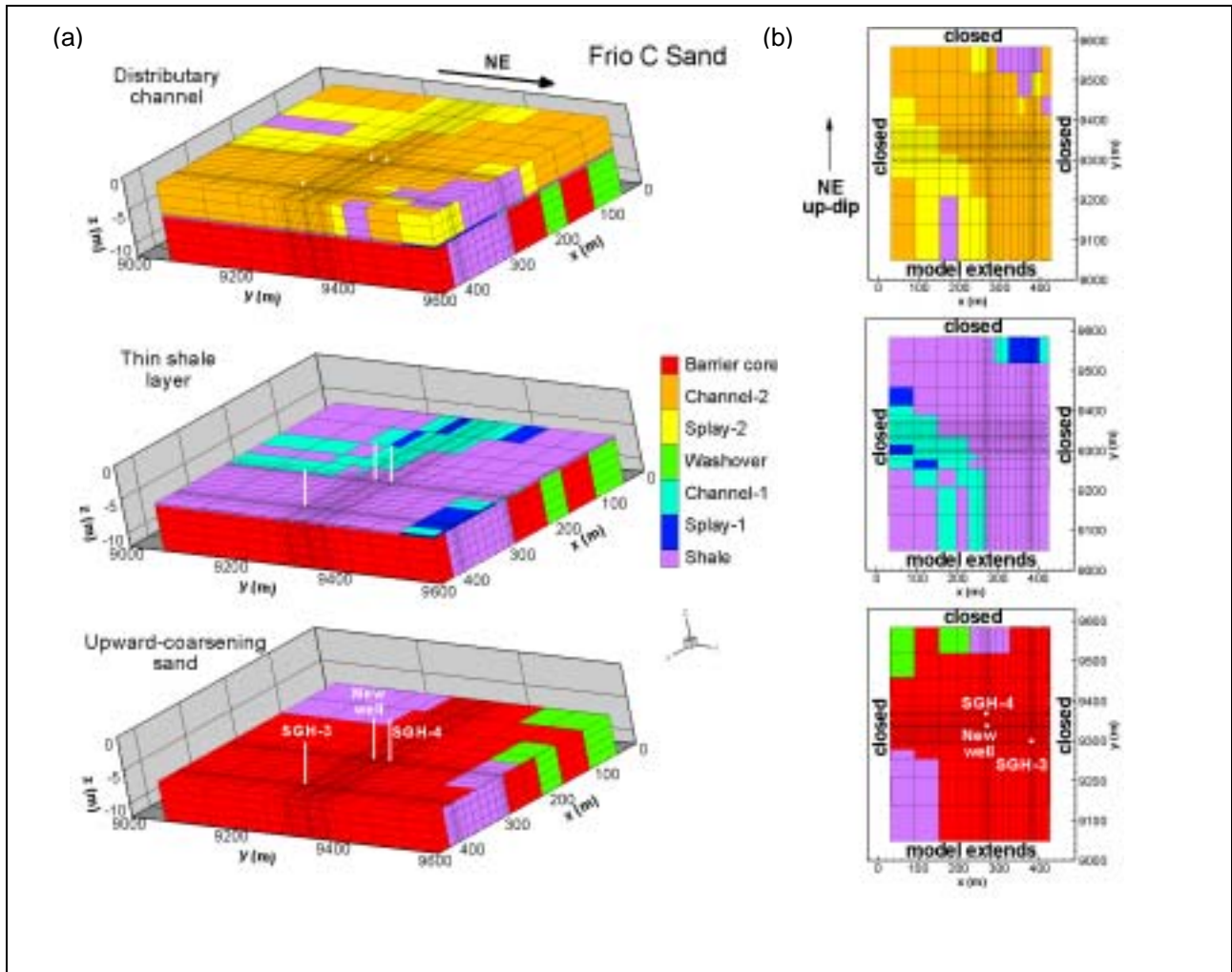

Figure 5. (a) Cut-away views of South Liberty model; (b) plan view of depositional settings.

SIMULATION RESULTS

For both models, we begin with single-phase liquid brine under hydrostatic, isothermal conditions, and inject supercritical CO_2 through a single injection well screened over the lower half of the model.

Umbrella Point Power Plant Model

Carbon dioxide is injected at a rate of 21.6 kg/s (680,000 metric tons per year) for a period of 20 years, then the system is monitored for an additional 80 years to watch the evolution of the CO_2 plume. This injection rate represents about half of the CO_2 output from a 1,000 MW gas-fired power plant. Initial formation conditions are $P = 188$ bars, $T = 78^{o}C$, and TDS = 100,000 ppm. Under these conditions, CO_2 has a density of 577 kg/m^3 and a viscosity of $4.4 \cdot 10^{-5}$ Pa$\cdot$s.

Figure 6 shows a time sequence of spatial distributions of CO_2 in the immiscible gas-like phase during the injection period. Strongly preferential flow occurs, as buoyant CO_2 finds gaps in the shale layers containing higher-permeability sands and moves into the upper half of the model.
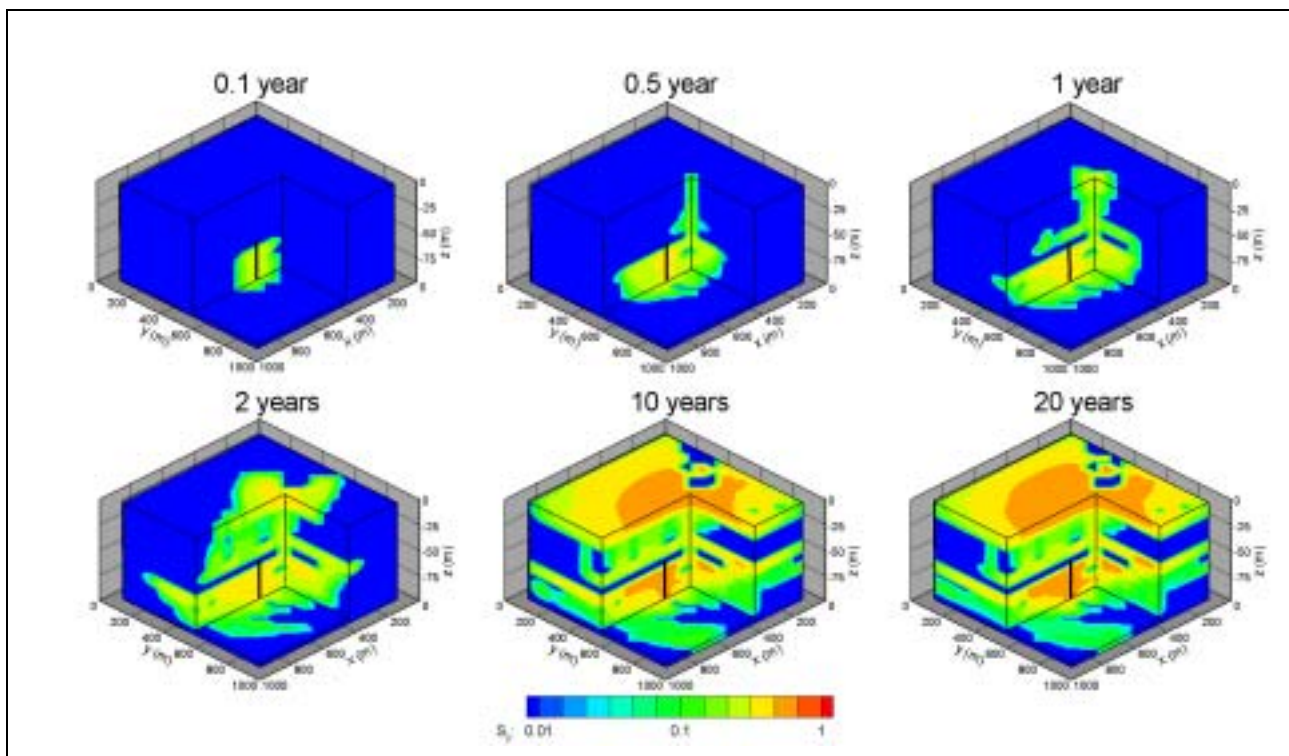

Figure 6. Spatial distributions of gas saturation S_g in basic Umbrella Point model during 20-year injection period.

Figure 7 shows the analogous time sequence for a model with a finer vertical grid in which there are three grid layers for each depositional layer. The overall patterns of plume development are similar for the coarse and fine grids, but the fine-grid model shows higher concentrations of CO_2 as it allows resolution of buoyancy flow within individual sand channels. Results (not shown) for a medium-grid model with two grid layers for each depositional layer are intermediate between Figures 6 and 7.

Comparison of Figures 6 and 7 shows that from two years on, the fine-grid model appears to contain more CO_2. To quantify CO_2 sequestration, we define the capacity factor C as the fraction of a specified volume of the subsurface containing CO_2. Capacity factor can be broken down by phase: $C = C_g + C_l$, where C_g is the fraction of the subsurface containing CO_2 in the gas-like phase and C_l is the fraction containing CO_2 dissolved in the aqueous phase. We have

$$C_g = <S_g\phi> \qquad\qquad (1)$$

$$C_l = <S_l\phi X_l^{CO2}(\rho_l/\rho_g)> \qquad\qquad (2)$$

where S_g and S_l are gas and liquid saturations, respectively, ϕ is porosity, X_l^{CO2} is the mass fraction of CO_2 dissolved in the aqueous phase, ρ_l and ρ_g are liquid- and gas-phase densities, respectively, and the angle brackets indicate an average over the specified volume. For the Umbrella Point model, the averaging volume is simply the model volume. For sequestration sites with no natural boundaries, defining the averaging volume may require careful deliberation to enable meaningful capacity comparisons to be made (Doughty et al., 2002).
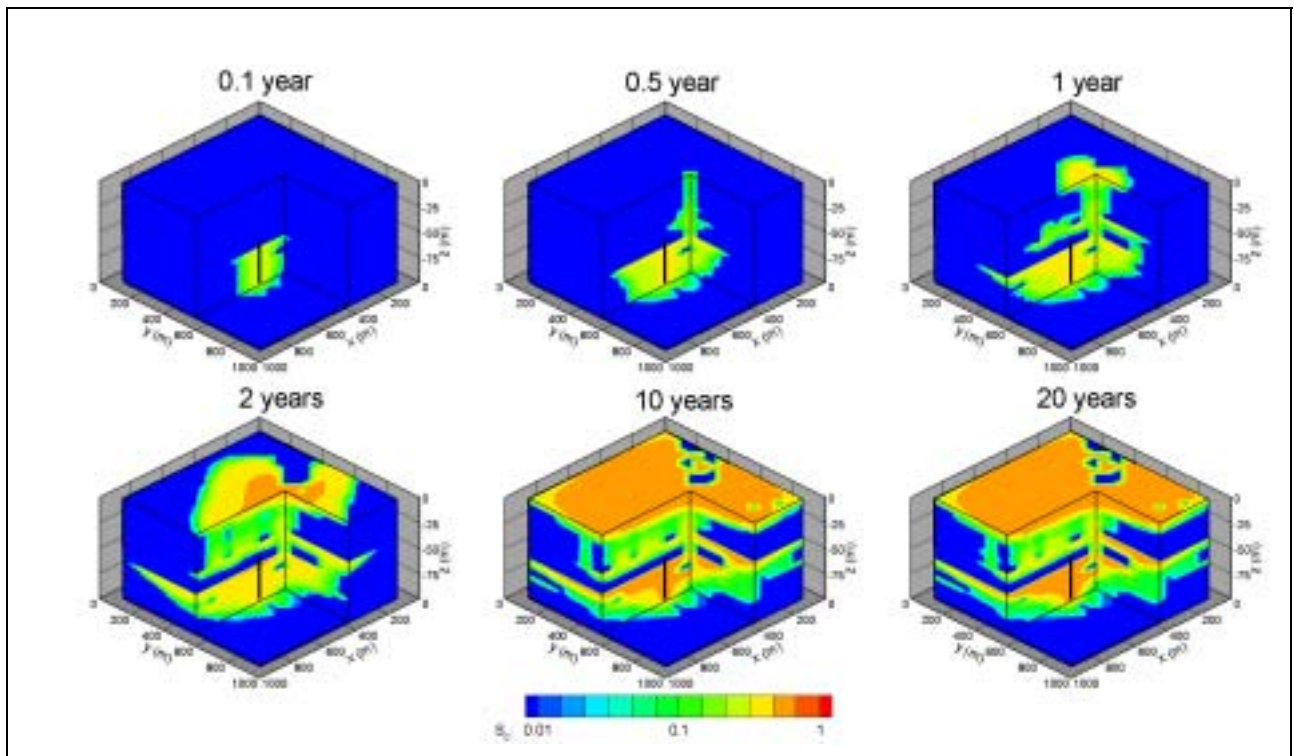

Figure 7. Spatial distributions of gas saturation S_g in fine-grid Umbrella Point model during 20-year injection period.

Figure 8 shows C versus time. Note that C increases linearly until the first CO_2 reaches the outer boundary of the model (the spill point) at about two years. By ten years, a quasi-steady state is reached in which the injection rate at the well nearly balances CO_2 flow out the lateral model boundaries. Note that between two and ten years, the amount of CO_2 stored in the model increases significantly, as buoyancy flow and heterogeneity interact to redistribute CO_2 throughout the model. This does not occur in a homogeneous model, and C increases only

slightly after the spill point is reached (Doughty et al., 2001). We define the capacity of the sequestration volume as the C value at the onset of quasi-steady conditions, but other authors have defined it using C at the spill point. As noted above, for homogeneous models, this choice makes little difference, whereas for the more realistic heterogeneous case considered here, it is quite significant, and the choice of when to evaluate C should be consistent with the conceptual model of the sequestration volume and its boundaries. Development of quasi-steady conditions by ten years indicates that the 1 km by 1 km modeled region is not large enough to store twenty years worth of CO_2 at the specified injection rate.

Figure 8a shows that C, C_g, and C_l are significantly smaller in the medium- and fine-grid models, where intra-sand channel buoyancy flow can be resolved and gas-like CO_2 becomes concentrated at the top of sand layers. Relative permeability effects then enable it to flow more readily to the open side boundaries of the model. Because the view of the model shown in Figures 6 and 7 is from above, the fine-grid model appears to contain more CO_2 when it actually contains less.

Figure 8b shows C_g and C_l for three stochastic realizations of the Umbrella Point model, each of which maintains the sequence of depositional layers shown in Figure 3. Although the spatial distributions of CO_2 (not shown) vary greatly among the models, reflecting different locations for shale layer gaps that promote preferential upward flow, the integrated measures provided by the capacity factors are quite similar.
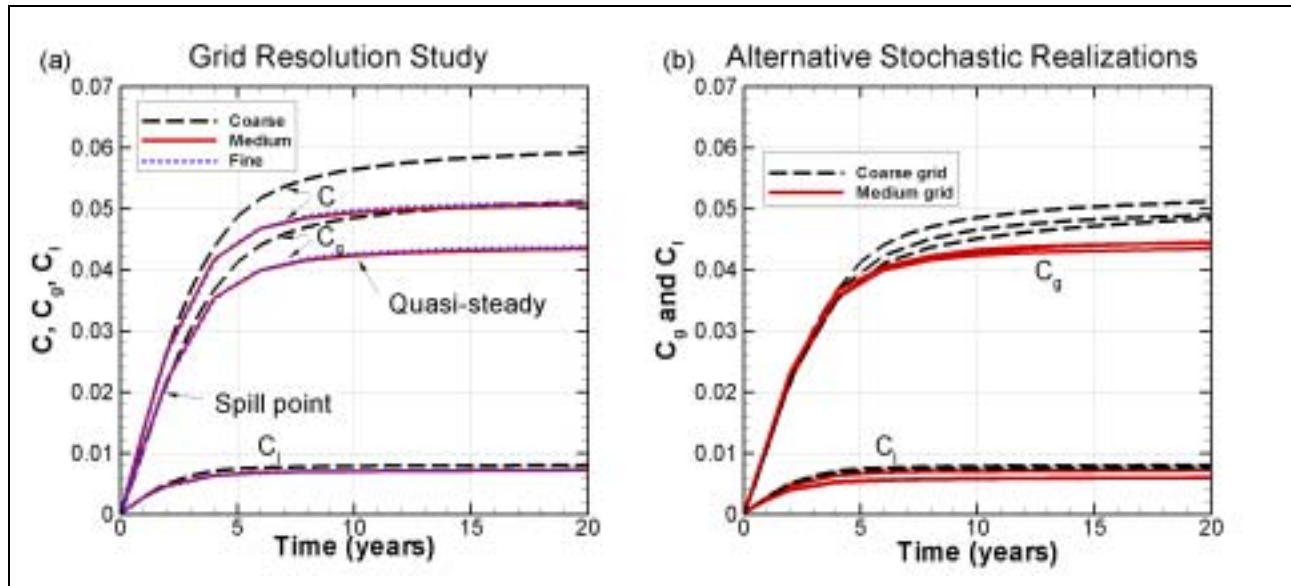

Figure 8. Capacity factor (fraction of subsurface containing CO_2) as a function of time during 20-year injection period: (a) grid resolution study (medium- and fine-grid models give nearly identical results); (b) alternative stochastic realizations for coarse- and medium-grid models.

South Liberty Pilot Site Model

Carbon dioxide is injected at a rate of 2.9 kg/s (250 metric tons per day) for a period of 20 days, then the simulation continues with no injection for one year to watch the evolution of the CO_2 plume. Initial formation conditions are $P = 150$ bars, $T = 64^{\circ}$C, and TDS = 100,000 ppm. Under these conditions, CO_2 has a density of 565 kg/m^3 and a viscosity of $4.3\cdot10^{-5}$ Pa·s. This injection schedule is comparable to what is planned for the pilot test, where the high costs of

trucked-in CO_2 and field time must be balanced against the goal of injecting enough CO_2 to be able to monitor it in the subsurface. In particular, there will be one monitoring well located about 30 m updip of the injection well (labeled "SGH-4" and "new well", respectively, in Figure 5). One of the tasks of numerical modeling is to predict when injected CO_2 will arrive at the monitoring well.

Figure 9 shows gas-phase CO_2 plume development for the basic South Liberty model with a sequence of plan views of the top of the upward-coarsening sand, which is the top of the injection interval. During the 20-day injection period, the distribution of CO_2 is nearly radially symmetric around the injection well, but after injection ends, the buoyant flow of CO_2 updip becomes obvious. After one year, the bulk of the plume has moved updip of both the injection and monitoring wells. The irregular shape at the leading edge of the one-year plume reflects flow around a shaley region (Figure 5).
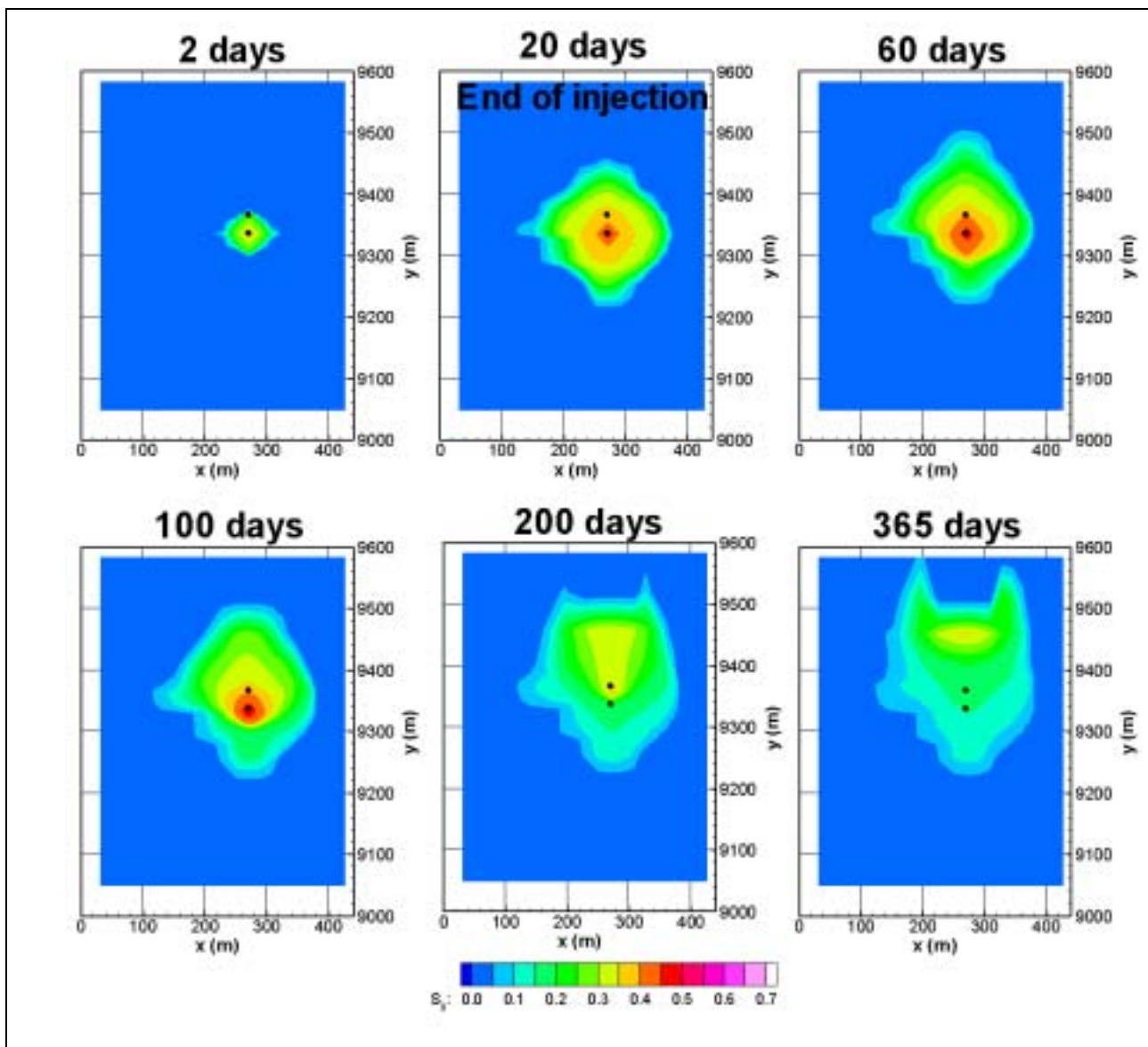
Figure 9. Time sequence of S_g distributions at top of upward-coarsening sand in South Liberty model, with five-point differencing, a non-uniform grid, and generic characteristic curves. Positive y-direction is updip; injection and monitoring wells are shown.

During the injection period, the plan view of the CO_2 plume actually looks more diamond-shaped than circular (Figure 9, first two frames). The model has homogeneous properties close to the injection well (Figure 5), so the lack of radial symmetry may be due to grid effects. To investigate the role of the grid, two alternative models were developed.

The diamond-shape of the early CO_2 plume is a hallmark of the preferential flow that typically arises along the axis directions in a rectangular grid that uses five-point differencing for lateral connections (i.e., four lateral connections for each grid block, one to each of its nearest neighbors). This problem can be ameliorated by using nine-point differencing for lateral connections (i.e., eight lateral connections for each grid block, the usual four nearest neighbors, plus the four nearest diagonal neighbors).

The implementation of nine-point differencing used here (K. Pruess, private communication, 1996) requires a laterally regular grid with square grid blocks. In the original grid, lateral spacing ranges from 2 m at the wells, to about 60 m near the closed edges of the model, to several hundred meters to the southwest, where the model extends far enough to act unbounded (Figure 5). A new grid with a uniform lateral spacing of 7.5 m was created. This grid will not resolve near-well behavior as well as the original grid and it has a constant-pressure boundary rather than extending far in the down-dip direction – a concession to size limitations of the computer being used for the simulations.

Figures 10 and 11 show plume development for the uniform grid with five-point and nine-point differencing for lateral connections, respectively. During the injection period, nine-point differencing produces a more circular plume, as expected. An unanticipated result is that during the post-injection period, the added lateral flow enabled by nine-point differencing slightly increases updip translation of the plume.
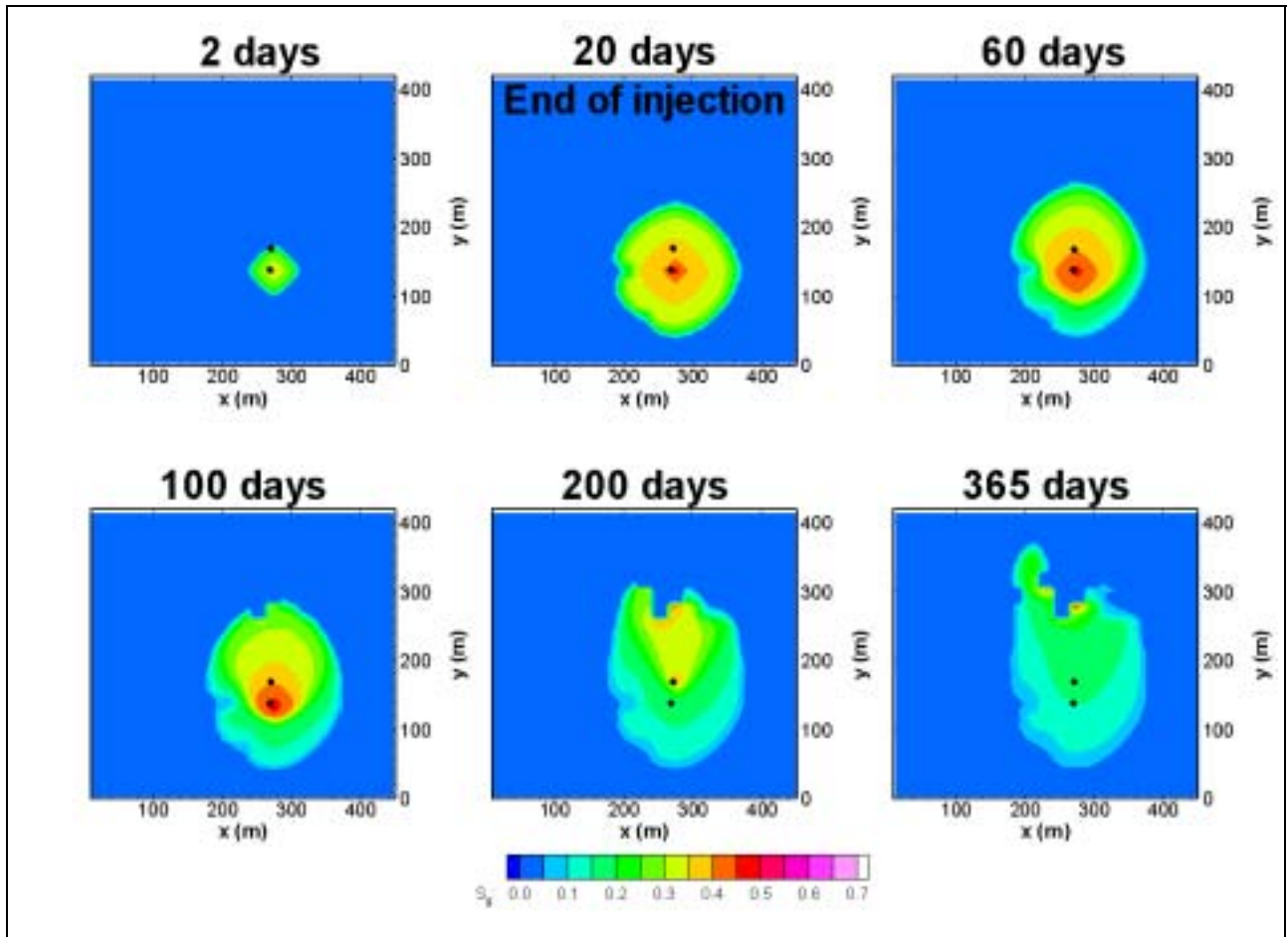
Figure 10. Time sequence of S_g distributions at top of upward-coarsening sand in South Liberty model with five-point differencing, a uniform grid, and generic characteristic curves.
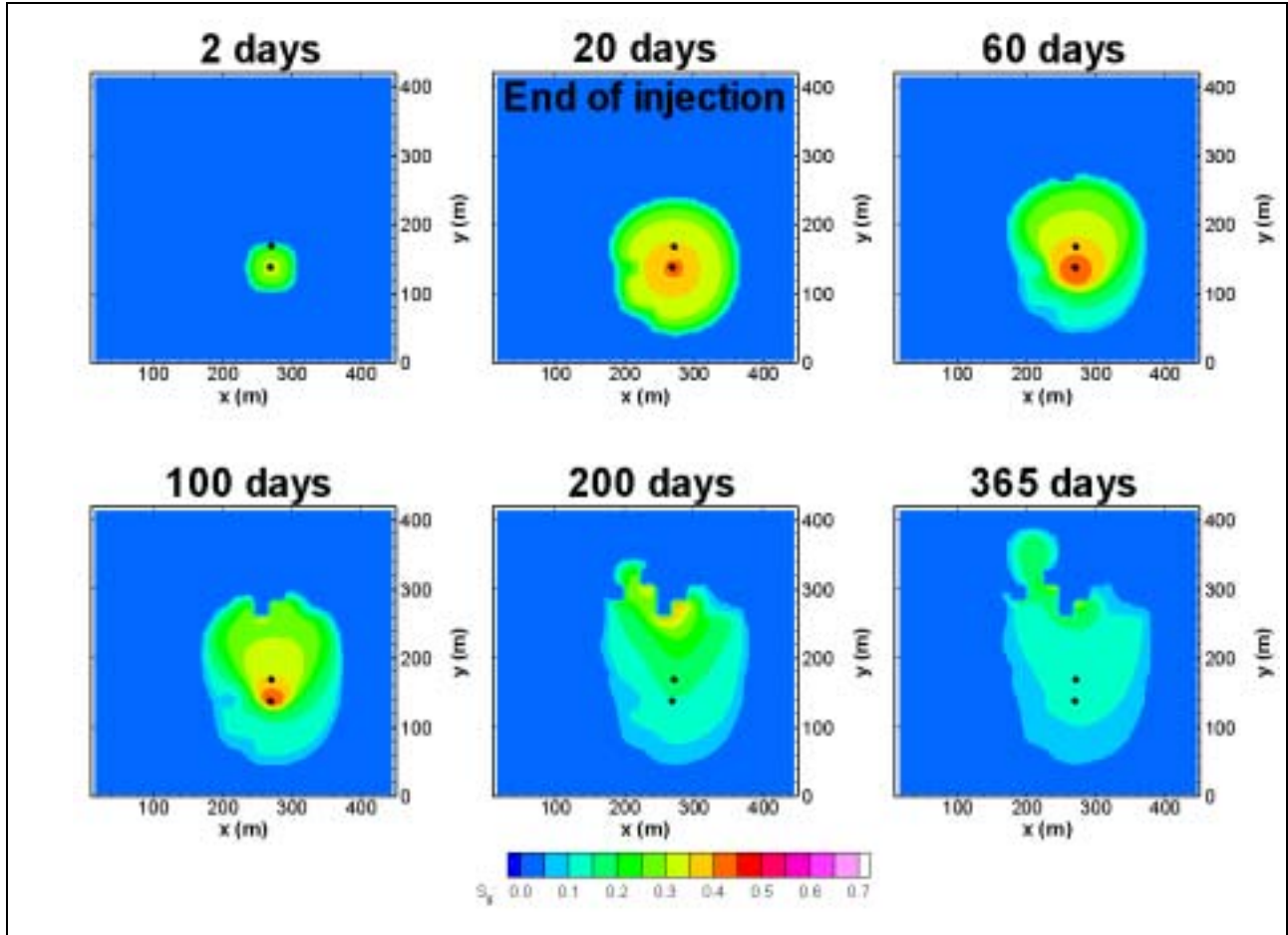
Figure 11. Time sequence of S_g distributions at top of upward-coarsening sand in South Liberty model with nine-point differencing, a uniform grid, and generic characteristic curves.

Comparison to the plume resulting from the non-uniform grid (Figure 9) makes it apparent that the preferential flow in the grid axis directions is exacerbated by the coarsening of the grid away from the wells, which further distorts the shape of the plume by enhancing spreading due to numerical dispersion. Spreading due to phase dispersion is an important aspect of plume evolution; it is undesirable to mask this process with spurious numerical effects. Moreover, with the more accurate plume depiction afforded by a finer grid, subtle irregularities in the plume shape may be attributed to geological features. In particular, the small indentations in the lower left quadrant of the plume, visible starting at 20 days, reflect gaps in the overlying thin shale layer, where CO_2 is leaking into the upper half of the model (see Figure 5).

Recent work involving a literature survey and core analyses (M. Holtz, private communication, 2002) has indicated that typical relative permeability curves for the sand facies of the Frio formation in the vicinity of the South Liberty field are rather different than the generic relative permeability curves used thus far. Figure 12 compares the generic curves and "Frio-like" curves adapted from Holtz' work. The generic curves use the van Genuchten (1980) functional form for liquid relative permeability k_{rl} and the Corey (1954) functional form for gas relative permeability k_{rg} whereas the Frio-like curves use Corey curves for each. The more significant distinction between the two sets of curves is the residual saturations used. The generic curves have a large residual liquid saturation S_{lr} and a small residual gas saturation S_{gr}

whereas the Frio-like curves have a small S_{lr} and a large S_{gr} (see Figure 12). The differences in residual saturation act to shift the Frio-like curves to the left. That is, over the entire range of saturation values, the Frio-like curves show greater liquid mobility and less gas mobility.
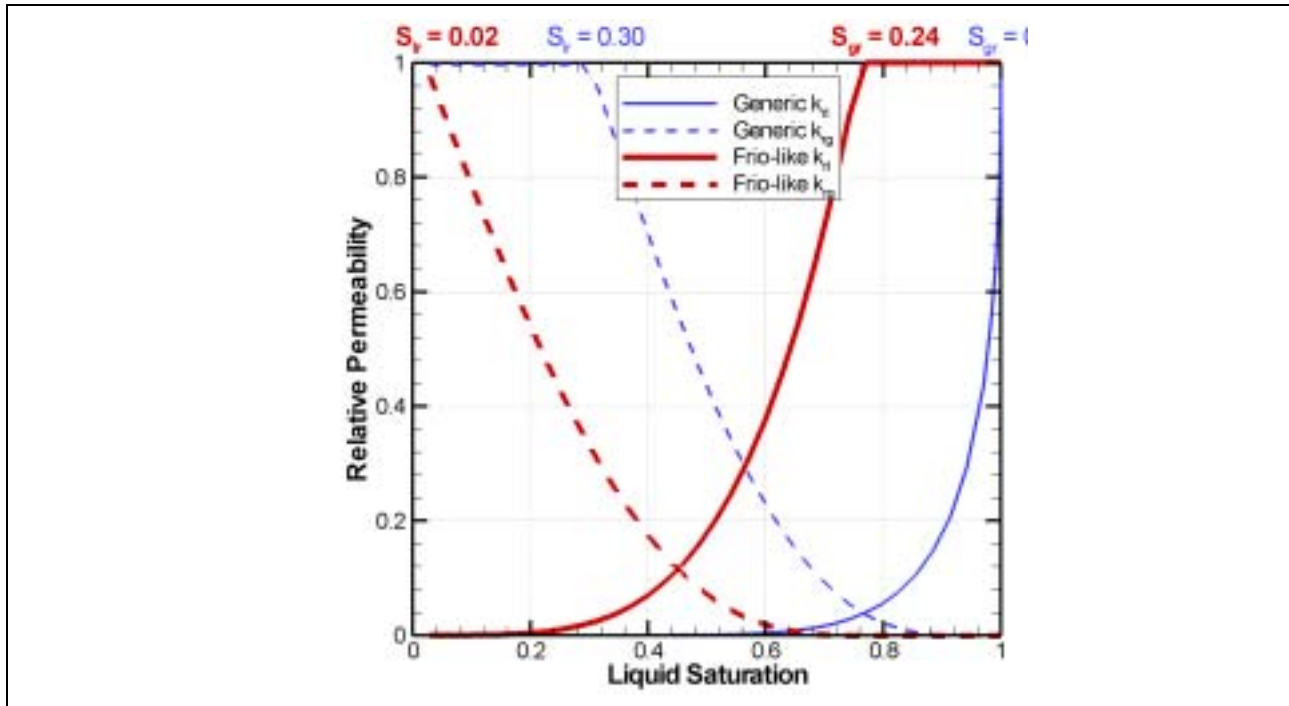

Figure 12. Relative permeability curves used for the South Liberty simulations.

Figure 13 shows plume development for the Frio-like characteristic curves. Compared to the case with generic characteristic curves (Figure 11), during the injection period, the gas-like CO_2 plume is much more compact (higher gas saturation and smaller radial extent). After injection ends, the plume begins to spread, and it does not take long for the gas saturation to decrease to the residual value, making the plume essentially immobile. Thus, the plume does not migrate nearly as far updip as for the generic characteristic curves, but remains localized near the injection well.

The differences in plume behavior for the different sets of characteristic curves have important ramifications for the pilot test. Choices about the timing, location, and sensitivity of monitoring techniques depend strongly on the nature of the CO_2 plume. For example, although the arrival time of the plume at the monitoring well does not depend too much on the choice of residual saturations (2-3 days in either case), the passage of the trailing edge certainly does. A series of geophysical surveys designed to image plume passage could be completed over the course of one year for the generic characteristic curves, but for the Frio-like characteristic curves the same series would show an essentially steady plume.
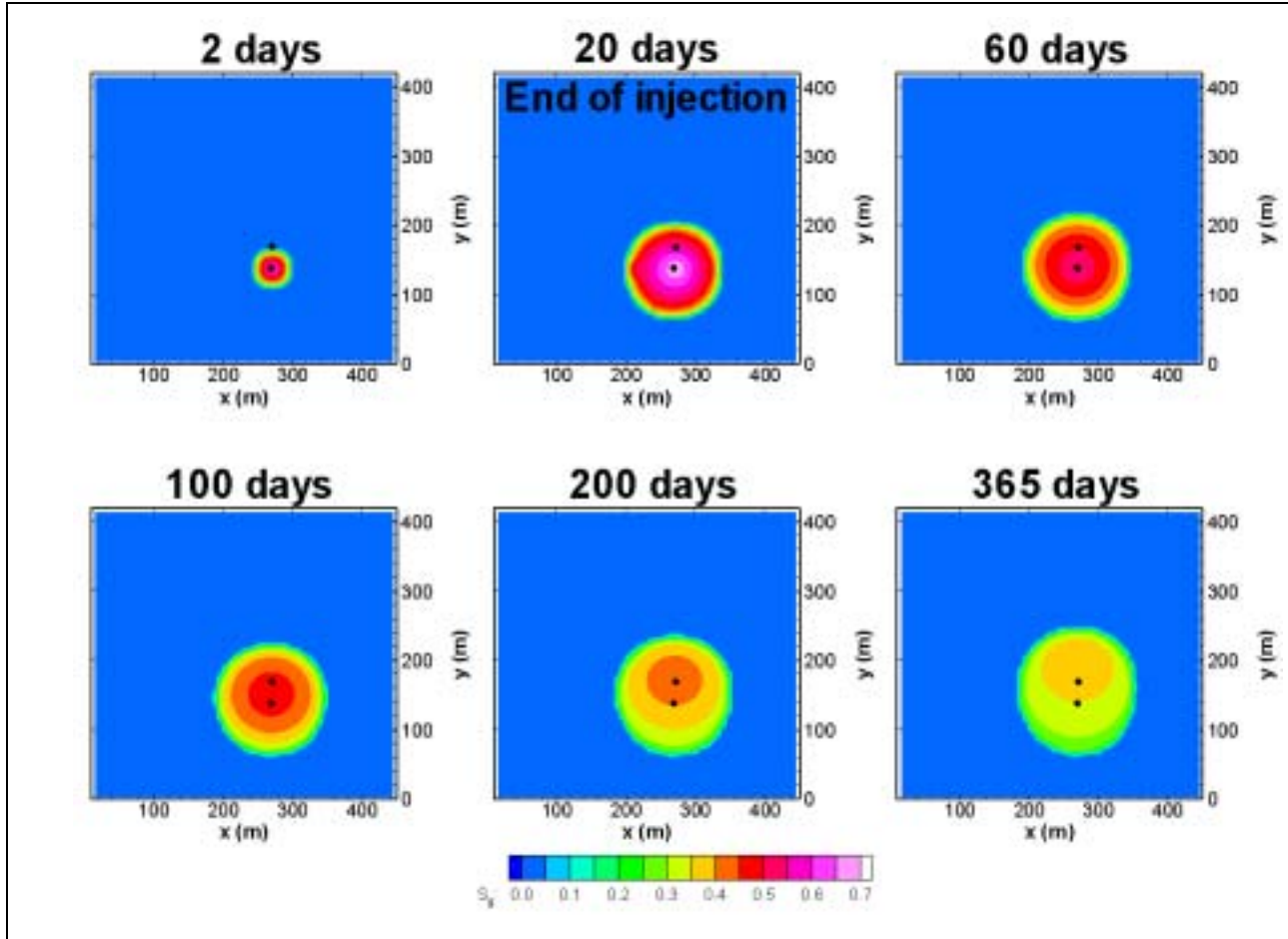
Figure 13. Time sequence of S_g distributions at top of upward-coarsening sand in South Liberty model with nine-point differencing, a uniform grid, and Frio-like characteristic curves.

CONCLUSIONS

Modeling the injection and storage of supercritical CO_2 in brine-bearing formations has provided valuable insights into flow and transport behavior and has proved useful for planning monitoring activities during the upcoming pilot test. Subtle interplays between physical and numerical effects can occur, requiring that model development choices be made with care. In particular, grid resolution and orientation effects can produce results that mimic and mask physical processes accompanying buoyant flow in multi-phase heterogeneous systems.

The present study has reiterated the well-known finding that the choice of characteristic curves is very important. In this case, it is the end points of the relative permeability curves, the residual saturations, that play a critical role by shifting the saturation range for which the CO_2 plume is mobile. A key issue regarding the feasibility of geologic sequestration in general is whether there is adequate capacity in the subsurface to store the extremely large quantities of CO_2 necessary to impact the global carbon balance. The typical gas saturation in the CO_2 plumes (i.e., the "concentration" of CO_2) varies by nearly a factor of two for the different characteristic curves employed – a significant effect. Moreover, with high residual gas saturation, sites that are not perfectly sealed become viable for sequestration, as moderate saturation decreases arising from phase dispersion cause the plume to become immobile.

In comparing the multi-phase flow aspects of supercritical CO_2 injection into deep brine formations with vadose-zone processes, certain differences become apparent. The most obvious is that in the vadose zone we typically encounter the displacement of the non-wetting phase (air) by the wetting phase (water), a process known as imbibition or wetting. Here, the initial development of the CO_2 plume primarily involves displacement of the wetting phase (brine) by the non-wetting phase (supercritical CO_2), a drying process. The post-injection CO_2 plume evolution shown for the South Liberty model also involves rewetting of rock by brine at the trailing edge of the plume as it moves upward and updip by buoyancy flow (analogously, the trailing edge of an infiltration pulse moving through the vadose zone represents a drying process). Comparison of Figures 9, 10, and 11 indicates that grid effects are important under both wetting and drying conditions, and thus are pertinent to a variety of vadose-zone processes.

An important distinction between the vadose-zone wetting process and the rewetting encountered here during post-injection plume movement is that typically in the vadose zone, the displacing fluid (infiltrating water) is not continuously applied for a long period of time, thus the overall liquid saturation remains low enough so that reductions in air permeability either need not be considered at all (the Richards Equation approximation), or are minor enough to represent with a relative permeability that has a small value of S_{gr} (see Figure 12). In contrast, our supercritical CO_2 plume represents a relatively small volume of non-wetting phase fluid, which makes non-wetting phase entrapment potentially significant, suggesting that a large value of S_{gr} is appropriate during rewetting. A noteworthy complication is that there is no real justification for using a large value of S_{gr} during the initial formation of the CO_2 plume, and in fact, a hysteretic relative permeability curve that uses a small S_{gr} for drying and a large S_{gr} for wetting is probably more physically sound (Finsterle et al., 1998; Holtz, 2002). Currently, we are investigating application of such a hysteretic relative permeability formulation to CO_2 injection in heterogeneous porous media. The lesson that the choice of residual saturations depends on the flow process is equally relevant to vadose-zone studies.

ACKNOWLEDGMENT

REFERENCES

Altunin, V.V., *Thermophysical properties of carbon dioxide* (in Russian), Publishing House of Standards, Moscow, 1975.

Battistelli, A., C. Calore, and K. Pruess, The simulator TOUGH2/EWASG for modeling geothermal reservoirs with brines and non-condensible gas, *Geothermics,* 26(4), 437-464, 1997.

Carle, S.F. and G.E. Fogg, Transition probability based indicator geostatistics, *Mathematical Geology,* 28(4), 453-477, 1996.

Carle, S.F. and G.E. Fogg, Modeling spatial variability with one and multidimensional continuous-lag Markov chains, *Mathematical Geology*, 29(7), 891-917, 1997.

Corey, A.T., The interrelation between gas and oil relative permeabilities, *Producers Monthly*, 38-41, November 1954.

Doughty, C., S.M. Benson, and K. Pruess, Capacity investigations of brine-bearing sands for geologic sequestration of CO_2, GHGT-6 Conference, Kyoto, Japan, September 30 – October 4, 2002.

Doughty, C., K. Pruess, S.M. Benson, S.D. Hovorka, P.R. Knox, and C.T. Green, Capacity investigation of brine-bearing sands of the Frio formation for geologic sequestration of CO_2, First National Conference on Carbon Sequestration, May 14-17, Washington DC, National Energy Technology Laboratory, 2001.

Finsterle, S., T.O. Sonenborg, and B. Faybishenko, Inverse modeling of a multistep outflow experiment for determining hysteretic hydraulic properties, in K. Pruess, ed., Proceedings of the TOUGH workshop '98, *Rep. LNBL-41995*, Lawrence Berkeley National Laboratory, Berkeley, Calif., 1998.

Fogg, G.E., S.F. Carle, and C.T. Green, A connected network paradigm for the alluvial aquifer system, in D. Zhang and C.L Winter, eds., Theory, modeling, and field investigation in hydrogeology: a special volume in honor of Shlomo P. Neuman's 60th birthday, Geol. Soc. of Am., Special Paper 348, 2001.

García, J.E. Fluid dynamics of carbon dioxide disposal into saline aquifers, PhD thesis, University of California at Berkeley, December 2003.

Galloway, W.E., Depositional architecture of Cenozoic gulf coastal plain fluvial systems, Circular 82-5, University of Texas at Austin, Bureau of Economic Geology, 1982.

Holtz, M. H., Residual gas saturation to aquifer influx: A calculation method for 3-D computer reservoir model construction (SPE 75502), SPE Gas Technology Symposium, Calgary, Alberta, Canada, 30 April-2 May, 2002.

Hovorka, S.D., C. Doughty, P.R. Knox, C.T. Green, K. Pruess, and S.M. Benson, Evaluation of brine-bearing sands of the Frio formation, upper Texas gulf coast for geological sequestration

of CO_2, First National Conference on Carbon Sequestration, May 14-17, Washington DC, National Energy Technology Laboratory, 2001.

Knox, P.R., C. Doughty, and S.D. Hovorka, Impacts of buoyancy and pressure gradient on field-scale geological sequestration of CO_2 in saline aquifers, AAPG Annual Meeting, Salt Lake City, May, 2003.

Pruess, K. and J. García, Multiphase flow dynamics during CO2 disposal into saline aquifers, *Environmental Geology*, 42, 282-295, 2002.

Pruess, K., C. Oldenburg, and G. Moridis, TOUGH2 user's guide, version 2.0, *Rep. LBNL-43134*, Lawrence Berkeley National Laboratory, Berkeley, Calif., 1999.

Pruess, K., T. Xu, J. Apps, and J. García, Numerical modeling of aquifer disposal of CO_2 (SPE 83695), *SPE Journal*, 49-60, March 2003.

van der Meer, L.G.H., The CO_2 storage efficiency of aquifers, *Energy Conservation and Management*, 36(6-9), 513-518, 1995.

van Genuchten, M.Th., A closed-form equation for predicting the hydraulic conductivity of unsaturated soils, *Soil Sci. Soc. Am. J.*, 44, 892-898, 1980.

Vining, M.R., Reserve growth in a mixed sequence of deltaic and barrier-island Frio sandstones, Umbrella Point field, Chambers County, Texas, *Gulf Coast Assoc. of Geol. Soc. Trans.*, 47, 611-619, 1997.

FIGURE CAPTIONS

Figure 1. Idealized representations of three fluvial depositional settings found in the Frio formation, used by TProGS to generate stochastic permeability fields.

Figure 2. Examples of the stochastic realizations produced by program TProGS. Each column shows three of the ten realizations created for a given depositional setting.

Figure 3. Well logs (Vining, 1997) and interpretation of sequence of depositional settings for Umbrella Point model (see Figure 4 for depositional-setting legend).

Figure 4. Cut-away view of Umbrella Point model. The injection well is shown as a black bar.

Figure 5. (a) Cut-away views of South Liberty model; (b) plan view of depositional settings.

Figure 6. Spatial distributions of gas saturation S_g in basic Umbrella Point model during 20-year injection period.

Figure 7. Spatial distributions of gas saturation S_g in fine-grid Umbrella Point model during 20-year injection period.

Figure 8. Capacity factor (fraction of subsurface containing CO_2) as a function of time during 20-year injection period: (a) grid resolution study (medium- and fine-grid models give nearly identical results); (b) alternative stochastic realizations for coarse- and medium-grid models.

Figure 9. Time sequence of S_g distributions at top of upward-coarsening sand in South Liberty model, with five-point differencing, a non-uniform grid, and generic characteristic curves. Positive y-direction is updip; injection and monitoring wells are shown.

Figure 10. Time sequence of S_g distributions at top of upward-coarsening sand in South Liberty model with five-point differencing, a uniform grid, and generic characteristic curves.

Figure 11. Time sequence of S_g distributions at top of upward-coarsening sand in South Liberty model with nine-point differencing, a uniform grid, and generic characteristic curves.

Figure 12. Relative permeability curves used for the South Liberty simulations.

Figure 13. Time sequence of S_g distributions at top of upward-coarsening sand in South Liberty model with nine-point differencing, a uniform grid, and Frio-like characteristic curves.

Table 1. Material properties for Umbrella Point model (Hovorka et al., 2001). For each depositional setting, framework facies is shown in bold (10^{-15} m^2 = 1 millidarcy).

Depositional Setting	Material	Permeability (10^{-15} m^2)	Porosity (%)
Barrier bar (B)	**Barrier core**	**700**	**32**
	Washover	200	29
	Shale	0.001	10
Distributary channel (D)	**Channel**	**400**	**30**
	Splay-2	250	30
	Shale	0.001	10
Interdistributary bayfill (BF)	Channel	400	30
	Splay-1	150	28
	Shale	**0.001**	**10**

Table 2. Material properties for South Liberty model (P. Knox, private communication, 2001). For each depositional setting, framework facies is shown in bold (10^{-15} m^2 = 1 millidarcy).

Depositional Setting	Material	Permeabililty (10^{-15} m^2)		Porosity (%)
		k_h	k_v	
Distributary Channel (D)	**Channel-2**	**286**	**114**	**28**
	Splay-2	78	31	21
	Shale	0.12	0.012	5
Thin shale layer (BF)	Channel-1	63	16	20
	Splay-1	17	4	15
	Shale	**0.12**	**0.012**	**5**
Upward-coarsening sand (B)	**Barrier core**	**63 - 286**	**16 - 191**	**20 - 28**
	Washover	17 - 78	4 - 52	15 - 21
	Shale	0.12	0.012	5